Localisation of stress-affected chemical reactions in solids described by coupled mechanics-diffusion-reaction models

Poluektov, Michael; Freidin, Alexander B.

Published in:
International journal of engineering science

DOI:
10.1016/j.ijengsci.2023.104006

Publication date:
2024

International Journal of Engineering Science 196 (2024) 104006

Contents lists available at ScienceDirect

International Journal of Engineering Science

journal homepage: www.elsevier.com/locate/ijengsci

Localisation of stress-affected chemical reactions in solids described by coupled mechanics-diffusion-reaction models

Michael Poluektov [a,*], Alexander B. Freidin [b]

[a] Department of Mathematical Sciences and Computational Physics, School of Science and Engineering, University of Dundee, Dundee, DD1 4HN, UK

[b] Institute for Problems in Mechanical Engineering of the Russian Academy of Sciences, 61 Bolshoy Pr., V.O., St. Petersburg, 199178, Russia

ARTICLE INFO

Keywords:
Chemo-mechanics
Stress-affected reactions
Stress-affected diffusion
Chemical affinity
Reaction locking
Phase-field method

ABSTRACT

Chemical reactions in solids can induce chemical expansion of the solid that causes the emergence of the mechanical stresses, which, in turn, can affect the rate of the reaction. A typical example of this is the reaction of Si lithiation, where the stresses can inhibit the reaction up to the reaction locking. The reactions in solids can take place within some volume (bulk reactions) or localise at a chemical reaction front (localised reactions). These cases are typically described by different thermo-chemo-mechanical theories that contain the source/sink terms either in the bulk or at the propagating infinitely-thin interface, respectively. However, there are reactions that can reveal both regimes; hence, there is a need to link the theories describing the bulk and the localised (sharp-interface) reactions. The present paper bridges this gap and shows that when a certain structure of the Helmholtz free energy density is adopted (based on the ideas from the phase-field methods), it is possible to obtain (in the limit) the same driving force for the chemical reaction (hence, the same reaction kinetics) as derived within the theory of the sharp-interface chemical reactions based on the chemical affinity tensor.

1. Introduction

The field of chemo-mechanics, which considers chemical reactions in deformable solids between solid and diffusive constituents, is currently undergoing an active development. This field aims at understanding problems such as lithiation of Si (McDowell et al., 2013b; de Vasconcelos et al., 2022) or self-limiting oxidation of Si (Büttner & Zacharias, 2006), which are accompanied by volumetric expansion of the solid reaction product that causes the emergence of the mechanical stress, which, in turn, affects the rate of the reaction. Chemo-mechanical modelling activities also focus on applications such as corrosion (Evstafeva & Pronina, 2023; Gutman, 1994; Pronina et al., 2018; Sedova & Pronina, 2022), swelling of temperature-sensitive gels (Drozdov, 2018), photochemical solidification of polymers during roll-to-roll nano-imprinting lithography (Gomez-Constante et al., 2021), solidification and glass transition of semi-crystalline polymers during additive manufacturing (Sreejith et al., 2023), fluid flow through the porous media with the temperature-dependent or the electric-field-dependent mass exchange between the phases (Ge et al., 2023; Soleimani et al., 2023), lithiation kinetics of electrode materials (Poluektov et al., 2018; Yang et al., 2023), diffusion-reaction processes in advecting membranes encountered in mechano-biology (Serpelloni et al., 2022), etc.

At the moment, this area of research is extensive, and above-mentioned examples and references cannot provide an exhaustive overview. The present study focuses only on modelling of some aspects of chemical reactions in solids, namely, consideration of localised and volumetric reactions from the unified point of view.

* Corresponding author.
E-mail address: mpoluektov001@dundee.ac.uk (M. Poluektov).

https://doi.org/10.1016/j.ijengsci.2023.104006
Received 7 December 2023; Accepted 10 December 2023
Available online 13 January 2024

Traditional macroscopic approach to reaction modelling consists in accounting for the source/sink terms in the mass balance equation governing the diffusive species (Glansdorff & Prigogine, 1971). Among more recent works, a distinction can be made between the mechano-diffusion, where the effect of mechanical stresses on the kinetics of the transport processes is investigated, e.g. Bower et al. (2011), Cui et al. (2012), Levitas and Attariani (2014) and Loeffel and Anand (2011), and consideration of mechanics-diffusion-reaction as three coupled processes. The latter theories can be separated into the stress-affected reactions taking place in a volume, e.g. Drozdov (2014), Knyazeva (2003), Loeffel et al. (2013) and Qin and Zhong (2021), and the stress-affected localised reactions, e.g. Cui et al. (2013), Freidin et al. (2014), Morozov et al. (2023) and Rao and Hughes (2000), which take place at a propagating interface (i.e. a chemical reaction front) between the chemically transformed and the untransformed phases. In the case of the localised reactions, the source/sink terms are at the propagating front that is usually assumed to be infinitely thin and is modelled as a sharp boundary. Although theories describing the volumetric and the localised reactions are typically pitched for different applications (i.e. different reactions), it is possible that the same reaction might reveal itself as either volumetric or localised. For example, the reaction of Si lithiation can take place both in the bulk and at the propagating front (McDowell et al., 2013a). For such reactions, ideally, a theory that captures both regimes is needed. In principle, the volumetric-reaction theories can be used to describe the localised reactions as well. For example, in Anguiano et al. (2022), the proposed thermodynamically-consistent thermo-chemo-mechanical theory with volumetrically-described reactions has been used to model the localised reaction of SiC oxidation by having a finite-width reaction zone where the bulk reaction takes place. However, the latter example has been limited to the case when the chemical reaction takes place much faster than diffusion, while, for example, the reaction of Si lithiation can localise under the opposite conditions — when the diffusion is much faster than the reaction rate (Liu et al., 2011). It is also known that some reactions should localise under certain conditions. For example, in Pronina (2017), Pronina and Khryashchev (2017), where mechanochemical dissolution of a material around an elliptical opening has been considered, formulas for the threshold loads corresponding to the transition from blunting to sharpening of the boundary at the ellipse vertices are given; this transition corresponds to localisation of corrosion.

The aim of the present paper is to eliminate the gap between the descriptions of the volumetric and the localised chemical reactions in deformable solids and to show that a volumetric reaction can localise and acquire in the limit the same stress-affected kinetics as a sharp-interface reaction. This is done by analysing the behaviour of the driving force for the chemical reactions — the chemical affinity. Therefore, first, the general thermo-chemo-mechanical theory governing the behaviour of a diffusive species within a deformable solid with the mass exchange between them is derived. This is followed by a comparison to the general theory governing the sharp-interface reactions, based on the chemical affinity tensor (Freidin, 2013). Finally, to demonstrate the applicability of the derived theory, a few computational examples are given.

2. Theory

An open system consisting of the deformable solid and the diffusing reactant, which diffuses through the solid and reacts with it, is considered. Such chemical reaction is described by the following chemical equation:

$$n_- B_- + n_* B_* \to n_+ B_+,$$

where B_- and B_+ are the untransformed and the transformed solid components, respectively, B_* is the diffusing reactant, n_-, n_* and n_+ are the stoichiometric coefficients. The chemical equation implies that n_- moles of the solid component should react with n_* moles of the diffusing reactant, leading to the so-called law of definite proportions:

$$\frac{\nu_- - \nu_-^0}{n_-} = \frac{\nu_* - \nu_*^0}{n_*} = -\frac{\nu_+ - \nu_+^0}{n_+}, \tag{1}$$

where $\nu_\pm^0$ and $\nu_\pm$ are the initial and the current number of moles, respectively, of the transformed and the untransformed solid components; ν_*^0 and ν_* are the initial and the current number of moles of the diffusing reactant, respectively. This allows introducing reaction extent ϕ. As will be seen later, it is convenient to introduce the reaction extent such that it is normalised, $\phi \in [0,1]$. When $\phi = 0$, the reaction has not started yet, while when $\phi = 1$ the reaction has been completed and the untransformed solid has become the transformed solid component, i.e. $\nu_- = 0$ and $\nu_+ = \nu_-^0 n_+ / n_-$. Thus,

$$\nu_- - \nu_-^0 = -a n_- \phi, \tag{2}$$

$$\nu_* - \nu_*^0 = -a n_* \phi, \tag{3}$$

where a is the normalisation coefficient and '$-$' in the right-hand side indicates that B_- and B_* are consumed. Coefficient a can be found from conditions at the reaction completion, i.e. $\phi = 1$, leading to $\nu_-^0 = a n_-$. This gives

$$a = \frac{m_-^0}{n_- M_-}, \tag{4}$$

where m_-^0 is the initial mass of the untransformed solid component and M_- is the molar mass of the untransformed solid component. This allows writing the change of mass of the diffusing reactant:

$$m_* - m_*^0 = M_* \left(\nu_* - \nu_*^0\right) = -\frac{m_-^0 n_* M_* \phi}{n_- M_-} = -\frac{\rho^0 V_0 n_* M_* \phi}{n_- M_-}, \tag{5}$$

where m_*^0 and m_* are the initial and the current masses of the diffusing reactant, respectively; M_* is the molar mass of the diffusing reactant; ρ^0 is the mass density of the untransformed solid component; V_0 is the volume of the untransformed solid component. Relation (5) will be used below to write the balance of mass of the diffusing reactant.

2.1. Balance of mass

The standard solid mechanics approach is employed, where the current and the reference configurations are considered. The balance laws are written with respect to the reference configuration of the body. Here, $\boldsymbol{F} = \left(\nabla_0 \boldsymbol{x}\right)^{\mathrm{T}}$ is the deformation gradient, which maps the reference configuration to the current configuration, and $\boldsymbol{x}$ is the current position vector of a material point as a function of position vector $\boldsymbol{X}$ of the point in the reference configuration and time t. The displacement is denoted as $\boldsymbol{u} = \boldsymbol{x} - \boldsymbol{X}$. The Nabla operator ∇_0 is defined with respect to the reference configuration. The volume change is denoted as $J = \det \boldsymbol{F}$.

Path-connected domain Ω in the reference configuration is considered. The reactant is diffusing through the domain; hence, its total mass can be written as

$$m_* = \int_\Omega \rho_*^0 \,\mathrm{d}\Omega, \tag{6}$$

where ρ_*^0 is the mass density of the diffusing reactant per unit volume of the reference configuration. The change of the total mass is due to the influx of the diffusing reactant through the boundary and due to the chemical reaction:

$$\frac{\mathrm{d}m_*}{\mathrm{d}t} = -\int_\Gamma \boldsymbol{j} \cdot \boldsymbol{N}_\Gamma \,\mathrm{d}\Gamma + \frac{\mathrm{d}}{\mathrm{d}t}\int_\Omega \zeta\phi \,\mathrm{d}\Omega, \tag{7}$$

where $\boldsymbol{j}$ is the diffusive flux of the diffusing reactant per unit surface of the reference configuration, $\Gamma = \partial\Omega$ is the boundary of domain Ω, vector $\boldsymbol{N}_\Gamma$ is the external normal to Γ, variable $\phi \in [0, 1]$ is the extent of the reaction. Diffusive flux $\boldsymbol{j}$ is by definition proportional to velocity $\boldsymbol{V}_*^0$ of the diffusing reactant with respect to the points of the reference configuration, $\boldsymbol{j} = \rho_*^0 \boldsymbol{V}_*^0$. Following Eq. (5), coefficient ζ is defined as

$$\zeta = -\frac{\rho^0 n_* M_*}{n_- M_-}, \tag{8}$$

where ρ^0 is the mass density of the solid per unit volume of the reference configuration. The molar concentration is defined as $c = \rho_*^0 / M_*$. Substituting the latter into Eq. (7) and rewriting it in the differential form results in the following mass balance equation:

$$M_* \dot{c} = -\nabla_0 \cdot \boldsymbol{j} + \zeta\dot{\phi}. \tag{9}$$

2.2. Balance of momentum

The change of the total linear momentum of the solid and the diffusing reactant within domain Ω is

$$\frac{\mathrm{d}}{\mathrm{d}t}\int_\Omega \left(\rho^0 \boldsymbol{v} + \rho_*^0 \boldsymbol{v}_*\right) \mathrm{d}\Omega = \int_\Gamma \left(\boldsymbol{P} + \boldsymbol{P}_* - \boldsymbol{v}_* \boldsymbol{j}\right) \cdot \boldsymbol{N}_\Gamma \,\mathrm{d}\Gamma + \int_\Omega \left(\rho^0 \boldsymbol{b} + \rho_*^0 \boldsymbol{b}_*\right) \mathrm{d}\Omega, \tag{10}$$

where $\boldsymbol{v}$ and $\boldsymbol{v}_*$ are the velocities of the points of the solid and the diffusing reactant, respectively, $\boldsymbol{P}$ and $\boldsymbol{P}_*$ are the first Piola–Kirchhoff stress tensors of the solid and the diffusing reactant, respectively, $\boldsymbol{b}$ and $\boldsymbol{b}_*$ are the volumetric forces acting on the solid and the diffusing reactant, respectively. The third term in the surface integral in Eq. (10) is the change of the momentum due to the influx of the diffusing reactant through the boundary. In the current configuration, the Cauchy stress tensor of the diffusing reactant is hydrostatic. When transformed to the reference configuration, the resulting first Piola–Kirchhoff stress tensor is $\boldsymbol{P}_* = -p_* J \boldsymbol{F}^{-\mathrm{T}}$, where p_* is the pressure of the diffusing reactant.

Rewriting Eq. (10) in the differential form results in

$$\rho^0 \dot{\boldsymbol{v}} + \dot{\rho}_*^0 \boldsymbol{v}_* + \rho_*^0 \dot{\boldsymbol{v}}_* = \nabla_0 \cdot \left(\boldsymbol{P}^{\mathrm{T}} + \boldsymbol{P}_*^{\mathrm{T}} - \boldsymbol{j}\boldsymbol{v}_*\right) + \rho^0 \boldsymbol{b} + \rho_*^0 \boldsymbol{b}_*. \tag{11}$$

The velocity of the diffusing reactant can be excluded from Eq. (11), since the velocity in the current configuration is related to the velocity in the reference configuration, which, in turn, is related to the diffusive flux:

$$\boldsymbol{v}_* - \boldsymbol{v} = \boldsymbol{F} \cdot \boldsymbol{V}_*^0 = \boldsymbol{F} \cdot \frac{\boldsymbol{j}}{\rho_*^0}. \tag{12}$$

Using the latter, the following is transformations can be made:

$$-\boldsymbol{j}\boldsymbol{v}_* = -\boldsymbol{j}\boldsymbol{F} \cdot \frac{\boldsymbol{j}}{M_* c} - \boldsymbol{j}\boldsymbol{v}, \tag{13}$$

$$\nabla_0 \cdot (-\boldsymbol{j}\boldsymbol{v}) = -\boldsymbol{v}\nabla_0 \cdot \boldsymbol{j} - \boldsymbol{j} \cdot \nabla_0 \boldsymbol{v} = \dot{\rho}_*^0 \boldsymbol{v} - \zeta\dot{\phi}\boldsymbol{v} - \boldsymbol{j} \cdot \dot{\boldsymbol{F}}^{\mathrm{T}}, \tag{14}$$

$$\dot{\rho}_*^0 \boldsymbol{v}_* + \rho_*^0 \dot{\boldsymbol{v}}_* = \dot{\boldsymbol{F}} \cdot \boldsymbol{j} + \boldsymbol{F} \cdot \dot{\boldsymbol{j}} + \dot{\rho}_*^0 \boldsymbol{v} + \rho_*^0 \dot{\boldsymbol{v}}, \tag{15}$$

where the mass balance equation has been used. Substituting the above into Eq. (11) results in

$$\left(\rho^0 + M_* c\right) \dot{\boldsymbol{v}} + 2\dot{\boldsymbol{F}} \cdot \boldsymbol{j} + \boldsymbol{F} \cdot \dot{\boldsymbol{j}} + \zeta\dot{\phi}\boldsymbol{v} = \nabla_0 \cdot \left(\boldsymbol{P}^{\mathrm{T}} + \boldsymbol{P}_*^{\mathrm{T}} - \frac{\boldsymbol{j}\boldsymbol{j}}{M_* c} \cdot \boldsymbol{F}^{\mathrm{T}}\right) + \rho^0 \boldsymbol{b} + M_* c \boldsymbol{b}_*. \tag{16}$$

2.3. Balance of energy

The change of the total energy of the solid and the diffusing reactant is

$$\begin{aligned}&\frac{\mathrm{d}}{\mathrm{d}t}\int_{\Omega}\left(\rho^0 u+\rho^0_* u_*+\frac{1}{2}\rho^0\boldsymbol{v}\cdot\boldsymbol{v}+\frac{1}{2}\rho^0_*\boldsymbol{v}_*\cdot\boldsymbol{v}_*\right)\mathrm{d}\Omega=\\&=\int_{\Gamma}\left(\boldsymbol{v}\cdot\boldsymbol{P}+\boldsymbol{v}_*\cdot\boldsymbol{P}_*-u_*\boldsymbol{j}-\frac{1}{2}\boldsymbol{v}_*\cdot\boldsymbol{v}_*\boldsymbol{j}-\boldsymbol{h}\right)\cdot\boldsymbol{N}_{\Gamma}\,\mathrm{d}\Gamma+\int_{\Omega}\left(\rho^0\boldsymbol{b}\cdot\boldsymbol{v}+\rho^0_*\boldsymbol{b}_*\cdot\boldsymbol{v}_*+\rho^0 r+\rho^0_* r_*\right)\mathrm{d}\Omega,\end{aligned}\tag{17}$$

where u and u_* are the internal energies per unit mass of the solid and the diffusing reactant, respectively, r and r_* are the internal heat sources per unit mass of the solid and the diffusing reactant, respectively, $\boldsymbol{h}$ is the heat flux. The surface integral in Eq. (17) consists of the rate of work of external load (applied to the solid and the diffusing reactant), the influx of the heat and the influx of the energy due to the diffusion. The energy itself consists of the internal energy and the kinetic energy.

Rewriting Eq. (17) in the differential form results in

$$\begin{aligned}&\dot{\rho}^0_* u_*+\frac{1}{2}\dot{\rho}^0_*\boldsymbol{v}_*\cdot\boldsymbol{v}_*+\rho^0\dot{u}+\rho^0_*\dot{u}_*+\rho^0\boldsymbol{v}\cdot\dot{\boldsymbol{v}}+\rho^0_*\boldsymbol{v}_*\cdot\dot{\boldsymbol{v}}_*=\left(\nabla_0\cdot\boldsymbol{P}^{\mathrm{T}}\right)\cdot\boldsymbol{v}+\left(\nabla_0\cdot\left(\boldsymbol{P}^{\mathrm{T}}_*-\boldsymbol{j}\boldsymbol{v}_*\right)\right)\cdot\boldsymbol{v}_*-\nabla_0\cdot\left(u_*\boldsymbol{j}\right)+\\&+\rho^0\boldsymbol{b}\cdot\boldsymbol{v}+\rho^0_*\boldsymbol{b}_*\cdot\boldsymbol{v}_*+\rho^0 r+\rho^0_* r_*-\nabla_0\cdot\boldsymbol{h}+\boldsymbol{P}:\nabla_0\boldsymbol{v}+\boldsymbol{P}_*:\nabla_0\boldsymbol{v}_*+\frac{1}{2}\boldsymbol{v}_*\cdot\boldsymbol{v}_*\nabla_0\cdot\boldsymbol{j}.\end{aligned}\tag{18}$$

Symbol ':' denotes the double inner product of two second-order tensors; in coordinate notation $\boldsymbol{A}:\boldsymbol{B}$ is $A_{ij}B_{ji}$. Using the balance of momentum, Eq. (11), to eliminate the volumetric forces results in

$$\begin{aligned}&\rho^0\dot{u}+\rho^0_*\dot{u}_*=\boldsymbol{P}^{\mathrm{T}}:\dot{\boldsymbol{F}}+\boldsymbol{P}_*:\nabla_0\boldsymbol{v}_*+\frac{1}{2}\boldsymbol{v}_*\cdot\boldsymbol{v}_*\left(\nabla_0\cdot\boldsymbol{j}+\dot{\rho}^0_*\right)-\nabla_0\cdot\left(u_*\boldsymbol{j}\right)+\\&+\rho^0 r+\rho^0_* r_*-\nabla_0\cdot\boldsymbol{h}-\dot{\rho}^0_* u_*-\left(\nabla_0\cdot\boldsymbol{P}^{\mathrm{T}}+\rho^0\boldsymbol{b}-\rho^0\dot{\boldsymbol{v}}\right)\cdot\frac{\boldsymbol{F}\cdot\boldsymbol{j}}{M_* c}.\end{aligned}\tag{19}$$

2.4. Entropy production

Assuming that the solid and the diffusing reactant are at the same temperature locally, the change of the entropy is

$$\frac{\mathrm{d}}{\mathrm{d}t}\int_{\Omega}\left(\rho^0 s+\rho^0_* s_*\right)\mathrm{d}\Omega\geq-\int_{\Gamma}\left(\frac{1}{T}\boldsymbol{h}+s_*\boldsymbol{j}\right)\cdot\boldsymbol{N}_{\Gamma}\,\mathrm{d}\Gamma+\int_{\Omega}\frac{\rho^0 r+\rho^0_* r_*}{T}\,\mathrm{d}\Omega,\tag{20}$$

where s and s_* are the entropies per unit mass of the solid and the diffusing reactant, respectively, T is the temperature. Similarly to the previous equations, the surface integral contains the influx of entropy due to the diffusion of the reactant.

Rewriting Eq. (20) in the differential form results in

$$\rho^0\dot{s}+\dot{\rho}^0_* s_*+\rho^0_*\dot{s}_*+\nabla_0\cdot\left(\frac{1}{T}\boldsymbol{h}\right)-\frac{\rho^0 r+\rho^0_* r_*}{T}+\nabla_0\cdot\left(s_*\boldsymbol{j}\right)\geq 0,\tag{21}$$

which after multiplication by T becomes

$$\rho^0 T\dot{s}+\dot{\rho}^0_* T s_*+\rho^0_* T\dot{s}_*+\nabla_0\cdot\boldsymbol{h}-\rho^0 r-\rho^0_* r_*-\boldsymbol{h}\cdot\frac{\nabla_0 T}{T}+T\nabla_0\cdot\left(s_*\boldsymbol{j}\right)\geq 0.\tag{22}$$

Using the balance of energy, Eq. (19), to eliminate the volumetric heat sources results in

$$\begin{aligned}&\rho^0 T\dot{s}+\dot{\rho}^0_* T s_*+\rho^0_* T\dot{s}_*-\rho^0\dot{u}-\rho^0_*\dot{u}_*-\dot{\rho}^0_* u_*-\boldsymbol{h}\cdot\frac{\nabla_0 T}{T}+T\nabla_0\cdot\left(s_*\boldsymbol{j}\right)-\nabla_0\cdot\left(u_*\boldsymbol{j}\right)+\\&+\boldsymbol{P}^{\mathrm{T}}:\dot{\boldsymbol{F}}+\boldsymbol{P}_*:\nabla_0\boldsymbol{v}_*+\frac{\boldsymbol{v}_*\cdot\boldsymbol{v}_*}{2}\left(\nabla_0\cdot\boldsymbol{j}+\dot{\rho}^0_*\right)-\left(\nabla_0\cdot\boldsymbol{P}^{\mathrm{T}}+\rho^0\boldsymbol{b}-\rho^0\dot{\boldsymbol{v}}\right)\cdot\frac{\boldsymbol{F}\cdot\boldsymbol{j}}{M_* c}\geq 0.\end{aligned}\tag{23}$$

After introducing $\psi=u-Ts$ and $\psi_*=u_*-Ts_*$ as the Helmholtz free energies per unit mass of the solid and of the diffusing reactant, respectively, and $f=\rho^0\psi+\rho^0_*\psi_*$ as the total Helmholtz free energy per unit volume of the reference configuration, the dissipation inequality becomes

$$\begin{aligned}&-\rho^0\dot{T}s-\rho^0_*\dot{T}s_*-\dot{f}-\left(\boldsymbol{h}+s_*T\boldsymbol{j}\right)\cdot\frac{\nabla_0 T}{T}-\boldsymbol{j}\cdot\nabla_0\psi_*+\psi_*\left(\dot{\rho}^0_*-\zeta\dot{\phi}\right)+\\&+\boldsymbol{P}^{\mathrm{T}}:\dot{\boldsymbol{F}}+\boldsymbol{P}_*:\nabla_0\boldsymbol{v}_*+\frac{\boldsymbol{v}_*\cdot\boldsymbol{v}_*}{2}\zeta\dot{\phi}-\left(\nabla_0\cdot\boldsymbol{P}^{\mathrm{T}}+\rho^0\boldsymbol{b}-\rho^0\dot{\boldsymbol{v}}\right)\cdot\frac{\boldsymbol{F}\cdot\boldsymbol{j}}{M_* c}\geq 0,\end{aligned}\tag{24}$$

where the mass balance equation has been used. The term with $\boldsymbol{P}_*$ can be rewritten as

$$\begin{aligned}&\boldsymbol{P}_*:\nabla_0\boldsymbol{v}_*=\boldsymbol{P}_*:\nabla_0\left(\boldsymbol{v}_*-\boldsymbol{v}\right)+\boldsymbol{P}_*:\nabla_0\boldsymbol{v}=-p_* J\boldsymbol{F}^{-\mathrm{T}}:\left(\nabla_0\boldsymbol{j}\cdot\boldsymbol{F}^{\mathrm{T}}\right)\frac{1}{\rho^0_*}-p_* J\boldsymbol{F}^{-\mathrm{T}}:\nabla_0\frac{\boldsymbol{F}}{\rho^0_*}\cdot\boldsymbol{j}-p_* J\boldsymbol{F}^{-\mathrm{T}}:\dot{\boldsymbol{F}}^{\mathrm{T}}=\\&=-\frac{p_* J}{M_* c}\nabla_0\cdot\boldsymbol{j}-\left(\frac{p_* J}{M_*}\boldsymbol{F}^{-\mathrm{T}}:\nabla_0\frac{1}{c}\boldsymbol{F}+\frac{p_* J}{M_* c}\boldsymbol{F}^{-\mathrm{T}}:\nabla_0\boldsymbol{F}\right)\cdot\boldsymbol{j}-p_*\dot{J}=\frac{p_* J}{M_* c}\left(\dot{\rho}^0_*-\zeta\dot{\phi}\right)-\left(\frac{p_* J}{M_*}\nabla_0\frac{1}{c}+\frac{p_*}{M_* c}\nabla_0 J\right)\cdot\boldsymbol{j}-p_*\dot{\boldsymbol{j}},\end{aligned}\tag{25}$$

where Eq. (12) and $\partial J/\partial\boldsymbol{F}=J\boldsymbol{F}^{-\mathrm{T}}$ have been used. The dynamic term can be rewritten as

$$\boldsymbol{v}_*\cdot\boldsymbol{v}_*=\left(\boldsymbol{v}+\boldsymbol{F}\cdot\boldsymbol{j}\frac{1}{M_* c}\right)\cdot\left(\boldsymbol{v}+\boldsymbol{F}\cdot\boldsymbol{j}\frac{1}{M_* c}\right)=\boldsymbol{v}\cdot\boldsymbol{v}+\frac{\boldsymbol{C}:\boldsymbol{j}\boldsymbol{j}}{M^2_* c^2}+2\frac{\boldsymbol{F}:\boldsymbol{j}\boldsymbol{v}}{M_* c},\tag{26}$$

where $\boldsymbol{C} = \boldsymbol{F}^{\mathrm{T}} \cdot \boldsymbol{F}$ is the right Cauchy–Green deformation tensor. After introducing $S = \rho^0 s + \rho^0_* s_*$ as the total entropy per unit volume of the reference configuration, $R = \rho^0 r + \rho^0_* r_*$ as the total heat source per unit volume of the reference configuration, $\boldsymbol{H} = \boldsymbol{h} + s_* T \boldsymbol{j}$ as the total heat flux, and $\mu_* = M_* \psi_* + p_* J/c$ as the chemical potential, the dissipation inequality becomes

$$\begin{aligned} &- S\dot{T} - \dot{f} - \boldsymbol{H} \cdot \frac{\nabla_0 T}{T} - \frac{1}{M_*} \boldsymbol{j} \cdot \left(\nabla_0 \mu_* - \frac{\boldsymbol{J}}{c} \nabla_0 p_* + \frac{1}{c} \boldsymbol{F}^{\mathrm{T}} \cdot \left(\nabla_0 \cdot \boldsymbol{P}^{\mathrm{T}} + \rho^0 \boldsymbol{b} - \rho^0 \dot{\boldsymbol{v}} \right) \right) + \\ &+ \mu_* \left(\dot{c} - \frac{1}{M_*} \zeta \dot{\phi} \right) + \boldsymbol{P}^{\mathrm{T}} : \dot{\boldsymbol{F}} - p_* \dot{J} + \frac{1}{2} \left(\boldsymbol{v} \cdot \boldsymbol{v} + \frac{\boldsymbol{C} : \boldsymbol{j}\boldsymbol{j}}{M_*^2 c^2} + 2 \frac{\boldsymbol{F} : \boldsymbol{j}\boldsymbol{v}}{M_* c} \right) \zeta \dot{\phi} \geq 0. \end{aligned} \tag{27}$$

Having obtained inequality (27), one can identify the entropy production due to the chemical reaction and introduce the scalar chemical affinity — the driving force for the chemical reaction. In case when f depends on ϕ, but not on $\nabla_0 \phi$, this has been demonstrated in, e.g. Poluektov and Figiel (2023) and Qin and Zhong (2021). However, to consider reaction localisation, the dependency on $\nabla_0 \phi$ should be introduced.

2.5. Two-phase material point

Since chemically transforming material is considered, it is reasonable to write the mechanical constitutive laws for the fully-transformed material and for the untransformed material. This creates a task of somehow combining these two dependencies into one constitutive law for material with some degree of chemical transformation. The latter can be done by considering a microscopic volume with some degree of transformation.

A representative volume element (RVE) consisting of the transformed and the untransformed phases is considered, Fig. 1. Within the RVE, the phases have spatially homogeneous deformation, the normal to the phase boundary is denoted as $\boldsymbol{N}$ and the volume fraction of the transformed phase is ϕ. Thus, reaction extent ϕ at material point $\boldsymbol{X}$ of the body (at the macroscopic scale) indicates the degree of the microstructural transformation at the point by the chemical reaction. Tensor $\boldsymbol{F}$, defined at the material point associated with the RVE, is the volume-average deformation gradient of the RVE:

$$\boldsymbol{F} = \phi \boldsymbol{F}_+ + (1 - \phi) \boldsymbol{F}_-. \tag{28}$$

The jump of the deformation gradient across the interface in the RVE has the same form (tensor product of a vector and the normal) as the jump of the deformation gradient in the case of a sharp interface:

$$[\![\boldsymbol{F}]\!] = \boldsymbol{F}_+ - \boldsymbol{F}_- = \boldsymbol{a}\boldsymbol{N}, \tag{29}$$

where vector $\boldsymbol{a}$ will be formally defined later. Normal $\boldsymbol{N}$, which is used within the RVE, comes from the macroscopic scale:

$$\boldsymbol{N} = -\frac{\nabla_0 \phi}{|\nabla_0 \phi|}. \tag{30}$$

Using the above, it is easy to see that

$$\boldsymbol{F}_+ = \boldsymbol{F} + (1 - \phi) \boldsymbol{a}\boldsymbol{N}, \tag{31}$$

$$\boldsymbol{F}_- = \boldsymbol{F} - \phi \boldsymbol{a}\boldsymbol{N}. \tag{32}$$

To the best knowledge of the authors, within the context of phase-field methods in application to solid mechanics, such split has been originally proposed in Schneider et al. (2015), where it has been formulated for linear elasticity, and in Schneider et al. (2017), where it has been reformulated for large deformations. The same split was later used for chemo-mechanics where the mechanical part was linear elastic (Tschukin et al., 2019).

Each deformation gradient can be multiplicatively decomposed into the mechanical and the non-mechanical parts:

$$\boldsymbol{F}_\pm = \boldsymbol{F}_{\pm \mathrm{M}} \cdot \boldsymbol{F}_{\pm \mathrm{C}}, \tag{33}$$

$$\boldsymbol{F}_{\pm \mathrm{C}} = \boldsymbol{F}_{\pm \mathrm{C}}(c, T), \tag{34}$$

where the non-mechanical part does not depend on the reaction extent or its gradient. This allows introducing the corresponding first Piola–Kirchhoff stress tensors $\boldsymbol{P}_+$ and $\boldsymbol{P}_-$ that are functionals of $\boldsymbol{F}_{+\mathrm{M}}$ and $\boldsymbol{F}_{-\mathrm{M}}$, respectively, as well as c and T, such that

$$\boldsymbol{P} = \phi \boldsymbol{P}_+ + (1 - \phi) \boldsymbol{P}_-, \tag{35}$$

where $\boldsymbol{P}$ acquires the physical meaning of the volume-average first Piola–Kirchhoff stress tensor of the RVE. Vector $\boldsymbol{a}$ that was introduced above can be obtained from the condition analogous to the traction continuity in the case of a sharp interface (as was proposed in Schneider et al., 2017):

$$\boldsymbol{P}_+ \cdot \boldsymbol{N} = \boldsymbol{P}_- \cdot \boldsymbol{N}. \tag{36}$$

The above relations can be substituted into the sixth term of inequality (27):

$$\boldsymbol{P}^{\mathrm{T}} : \dot{\boldsymbol{F}} = \phi \boldsymbol{P}_+^{\mathrm{T}} : \dot{\boldsymbol{F}}_+ + (1 - \phi) \boldsymbol{P}_-^{\mathrm{T}} : \dot{\boldsymbol{F}}_- + \dot{\phi} \boldsymbol{P} : [\![\boldsymbol{F}]\!]^{\mathrm{T}} - \phi (1 - \phi) [\![\boldsymbol{P}]\!] : [\![\dot{\boldsymbol{F}}]\!]^{\mathrm{T}}, \tag{37}$$

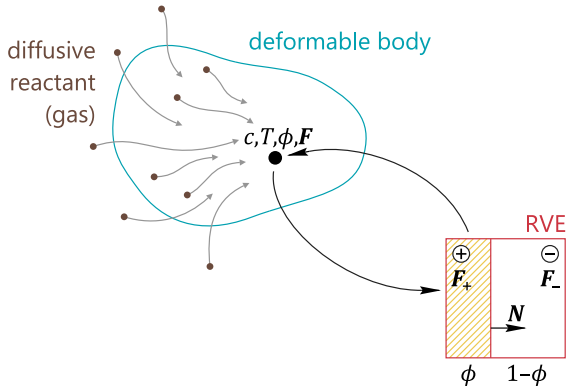

Fig. 1. The schematic illustration of a chemo-mechanical problem with the two-scale split into the macroscopic domain and the RVE.

where the last term transforms as

$$[\![\boldsymbol{P}]\!] : [\![\dot{\boldsymbol{F}}]\!]^{\mathrm{T}} = [\![\boldsymbol{P}]\!]^{\mathrm{T}} : \boldsymbol{a}\dot{\boldsymbol{N}}. \tag{38}$$

Following the idea that the quantities at a point are the volume-averages of the quantities of the RVE, the Helmholtz free energy density can be written as

$$f = \phi W_{+} + (1-\phi) W_{-} + W_{*} + f_{\mathrm{C}}, \tag{39}$$

where it is split between the mechanical part, which consists of the energies of the transformed and the untransformed solid phases, taken with the corresponding volume fractions, the energy of the diffusing reactant and the non-mechanical part. The latter, in general, depends on the reaction extent and its gradient, as well as the concentration and the temperature:

$$f_{\mathrm{C}} = f_{\mathrm{C}}\left(c, T, \phi, \nabla_0 \phi\right). \tag{40}$$

However, to model the localised reactions, one generalisation is necessary — a new microstructural field variable ξ is introduced, and it is assumed that the reaction extent is a function of this variable, $\phi = \phi(\xi)$. In the most simple setting, $\phi = \xi$ might be taken. A more complex dependence $\phi(\xi)$ will allow the existence of two stable domains, with $\phi = 0$ and $\phi = 1$, and the precise mechanism of this will be shown in Section 3. Thus, the non-mechanical part of the energy can be rewritten with the use of ξ:

$$f_{\mathrm{C}} = f_{\mathrm{C}}\left(c, T, \xi, \nabla_0 \xi\right). \tag{41}$$

Eqs. (37) and (39) can be substituted into inequality (27) resulting in

$$\begin{aligned} &- S\dot{T} - \boldsymbol{H} \cdot \frac{\nabla_0 T}{T} - \frac{\boldsymbol{j}}{M_*} \cdot \left(\nabla_0 \mu_* - \frac{\boldsymbol{J} \nabla_0 p_*}{c} + \frac{\boldsymbol{F}^{\mathrm{T}}}{c} \cdot \left(\nabla_0 \cdot \boldsymbol{P}^{\mathrm{T}} + \rho^0 \boldsymbol{b} - \rho^0 \dot{\boldsymbol{v}} \right) \right) + \mu_* \dot{c} - \phi \dot{W}_{+} - (1-\phi)\dot{W}_{-} - \dot{W}_{*} - \dot{f}_{\mathrm{C}} - p_* \dot{J} + \\ &+ \phi \boldsymbol{P}_{+}^{\mathrm{T}} : \dot{\boldsymbol{F}}_{+} + (1-\phi)\boldsymbol{P}_{-}^{\mathrm{T}} : \dot{\boldsymbol{F}}_{-} + \dot{\phi}\left(-\frac{\mu_* \zeta}{M_*} - [\![W]\!] + \boldsymbol{P} : [\![\boldsymbol{F}]\!]^{\mathrm{T}} + \frac{\boldsymbol{v}\cdot\boldsymbol{v}}{2}\zeta + \frac{\boldsymbol{C} : \boldsymbol{jj}}{2M_*^2 c^2}\zeta + \frac{\boldsymbol{F} : \boldsymbol{jv}}{M_* c}\zeta \right) - \\ &- \phi(1-\phi)[\![\boldsymbol{P}]\!]^{\mathrm{T}} : \boldsymbol{a}\dot{\boldsymbol{N}} \geq 0 \end{aligned} \tag{42}$$

Finally, the following quantities can also be substituted into inequality (42): the time derivative of f_{C},

$$\dot{f}_{\mathrm{C}} = \frac{\partial f_{\mathrm{C}}}{\partial c}\dot{c} + \frac{\partial f_{\mathrm{C}}}{\partial T}\dot{T} + \frac{\partial f_{\mathrm{C}}}{\partial \xi}\dot{\xi} + \frac{\partial f_{\mathrm{C}}}{\partial \nabla_0 \xi} \cdot \nabla_0 \dot{\xi}, \tag{43}$$

derivatives of ϕ,

$$\dot{\phi} = \frac{\partial \phi}{\partial \xi}\dot{\xi}, \qquad \nabla_0 \phi = \frac{\partial \phi}{\partial \xi}\nabla_0 \xi, \tag{44}$$

and the last term with the time derivative of $\boldsymbol{N}$,

$$[\![\boldsymbol{P}]\!]^{\mathrm{T}} : \boldsymbol{a}\dot{\boldsymbol{N}} = -[\![\boldsymbol{P}]\!]^{\mathrm{T}} : \boldsymbol{a}\left|\nabla_0 \phi\right|^{-1} \nabla_0 \dot{\phi} = -[\![\boldsymbol{P}]\!]^{\mathrm{T}} : \boldsymbol{a}\left|\nabla_0 \xi\right|^{-1} \nabla_0 \dot{\xi}. \tag{45}$$

2.6. Towards localised reactions

In thermodynamics of irreversible processes, the terms of the dissipation inequality are viewed as the products of the thermodynamic forces and the corresponding thermodynamic fluxes. Such structure allows assuming specific constitutive relations, where the fluxes are the functions of the forces, such that the dissipation inequality is always fulfilled (Glansdorff & Prigogine, 1971). Inequality (42) contains two terms related to the reaction extent (expressed via microstructural field variable ξ): one containing $\dot{\xi}$

and another containing $\nabla_0\dot{\xi}$, but $\dot{\xi}$ and $\nabla_0\dot{\xi}$ are not independent thermodynamic fluxes. The latter term can be transformed into the term with $\dot{\xi}$, thereby leading to the structure of the inequality that can be used for relating the reaction rate with the corresponding driving force.

Terms related to $\nabla_0\dot{\xi}$ in inequality (42) can be collected into $-\boldsymbol{q}\cdot\nabla_0\dot{\xi}$, where

$$\boldsymbol{q} = \frac{\partial f_{\mathrm{C}}}{\partial \nabla_0 \xi} - \phi(1-\phi)\,\boldsymbol{a}\cdot[\![\boldsymbol{P}]\!]\left|\nabla_0\xi\right|^{-1}. \tag{46}$$

It should also be reminded that inequality (42) is the differential form of the dissipation inequality, i.e. it is valid at all points of the body.

From this point onwards, reactions taking place in a 'thin' reaction zone are considered. This implies that outside of the reaction zone, $\dot{\xi}$ is negligibly small. The 'thin' reaction zone can be represented by the central surface and the thickness direction, which is chosen to be aligned with vector $\boldsymbol{q}$. Arbitrary area Σ that belongs to the central surface is considered. For each point of Σ, the set of all points along the thickness direction is denoted as τ. At this point, one can perform integration over the volume of the reaction zone $\Lambda = \Sigma\times\tau$ as the integration over surface Σ and thickness τ, assuming that the reaction zone is thin enough for its volume element to be approximated by $\mathrm{d}\Sigma\,\mathrm{d}\tau$. Considering the terms from inequality (42) that are related to $\nabla_0\dot{\xi}$ results in

$$\begin{aligned}
&-\int_\Lambda \boldsymbol{q}\cdot\nabla_0\dot{\xi}\,\mathrm{d}\Lambda = -\int_\Sigma\int_\tau \boldsymbol{q}\cdot\nabla_0\dot{\xi}\,\mathrm{d}\tau\,\mathrm{d}\Sigma = \\
&= \int_\Sigma\int_\tau \dot{\xi}\nabla_0\cdot\boldsymbol{q}\,\mathrm{d}\tau\,\mathrm{d}\Sigma - \int_\Sigma\int_\tau \nabla_0\cdot\left(\boldsymbol{q}\dot{\xi}\right)\mathrm{d}\tau\,\mathrm{d}\Sigma = \int_\Sigma\int_\tau \dot{\xi}\nabla_0\cdot\boldsymbol{q}\,\mathrm{d}\tau\,\mathrm{d}\Sigma - \int_\Gamma \boldsymbol{N}_\Gamma\cdot\boldsymbol{q}\dot{\xi}\,\mathrm{d}\Gamma,
\end{aligned} \tag{47}$$

where Γ is the external boundary of domain Λ. Surface Γ consists of sections of the external boundary of the reaction zone, on which $\dot{\xi}$ is negligibly small, and sections that cut across the reaction zone along $\boldsymbol{q}$, on which $\boldsymbol{N}_\Gamma$ is orthogonal to $\boldsymbol{q}$. Therefore, the surface integral in the right-hand side of Eq. (47) can be neglected. Finally, since Σ is arbitrary, Eq. (47) results in

$$-\int_\tau \boldsymbol{q}\cdot\nabla_0\dot{\xi}\,\mathrm{d}\tau = \int_\tau \dot{\xi}\nabla_0\cdot\boldsymbol{q}\,\mathrm{d}\tau.$$

Integrating inequality (42) over τ and substituting the above, gives the entropy production over the thickness of the reaction zone at a certain point of the central surface of the reaction zone.

The resulting dissipation inequality should be fulfilled under various different thermodynamic paths. Therefore, it is typically split into stronger relations — the so-called Coleman–Noll procedure (Coleman & Noll, 1963). In general, the dissipation might be due to the heat conduction, irreversible mechanical processes (e.g. plasticity or damage), the reactant diffusion and the chemical reaction. It is reasonable to assume that it is possible to recreate each irreversible thermodynamic process separately, which leads to a set of stronger inequalities dictating that the dissipation due to each thermodynamic process is non-negative. It is easy to see that the dissipation due to the chemical reaction becomes

$$\int_\tau A\dot{\xi}\,\mathrm{d}\tau \geq 0, \tag{48}$$

where A is the scalar chemical affinity expressed as

$$\begin{aligned}
A = \frac{\partial\phi}{\partial\xi}\left(-\frac{\mu_*\zeta}{M_*} - [\![W]\!] + \boldsymbol{P}:[\![\boldsymbol{F}]\!]^{\mathrm{T}} + \frac{1}{2}\boldsymbol{v}\cdot\boldsymbol{v}\zeta + \frac{1}{2}\frac{\boldsymbol{C}:\boldsymbol{jj}}{M_*^2c^2}\zeta + \frac{\boldsymbol{F}:\boldsymbol{jv}}{M_*c}\zeta\right) - \frac{\partial f_{\mathrm{C}}}{\partial\xi} + \\
+\nabla_0\cdot\left(\frac{\partial f_{\mathrm{C}}}{\partial\nabla_0\xi} - \phi(1-\phi)\,\boldsymbol{N}\cdot[\![\boldsymbol{F}]\!]^{\mathrm{T}}\cdot[\![\boldsymbol{P}]\!]\left|\nabla_0\xi\right|^{-1}\right).
\end{aligned} \tag{49}$$

It should be emphasised that inequality (48) is fulfilled if

$$A\dot{\xi} \geq 0. \tag{50}$$

The obtained inequality motivates choosing a constitutive law for reaction rate $\omega = \dot{\phi} = (\partial\phi/\partial\xi)\,\dot{\xi}$ as a function of the driving force for the chemical reaction — the scalar chemical affinity, i.e. $\omega = \omega(A)$.

It should be noted that expression (49) excludes surface effects, such as the surface tension, which can be naturally included by extending the description with strain-gradient terms, e.g. Eremeyev et al. (2019).

2.7. Comparison with the sharp-interface theory

The purpose of this section is to compare two different theories — the case of the volumetric reactions described in the present paper and the theory of the sharp-interface reactions developed in Freidin (2013), Freidin et al. (2014). In the latter case, the reactions take place at an interface (a chemical reaction front), which separates the chemically transformed phase and the untransformed phase. As the reaction proceeds, the reaction front moves through the domain of the considered deformable body, consuming the reactant that is diffusing through the transformed phase.

In the case of volumetric reactions, somewhat similar scenario can also occur — reaction localisation, when the reaction extent is either close to 1 or 0 within domain Ω, with a narrow transition region between the subdomains. This can happen due to the competition between $\nabla_0\xi$ term and the term dependent on ξ (e.g. a double-well potential) in the Helmholtz free energy density.

2.7.1. Localisation of a volumetric reaction

The simplest case to consider is a 1D profile of ξ. This will not give the full comparison between the theories, but will provide sufficient details to highlight the similarities and the differences. The starting point is to assume that the reaction has already localised due to $\nabla_0\xi$ and to consider the following approximate profile of the microstructural variable:

$$\xi = \begin{cases} 1, & X \le X_\mathrm{F} - 1/2\alpha, \\ -\alpha\left(X - X_\mathrm{F}\right) + 1/2, & \left|X - X_\mathrm{F}\right| < 1/2\alpha, \\ 0, & X \ge X_\mathrm{F} + 1/2\alpha, \end{cases} \tag{51}$$

where $X_\mathrm{F} = X_\mathrm{F}(t)$ is the position of the centre of the transition region, α is the slope, $1/\alpha$ is the width of the transition region. The transformed phase is to the left of the transition region, while the untransformed phase is to the right. In this case, $V_\mathrm{F} = \dot{X}_\mathrm{F}$ is the velocity with which the transition region moves through the material. Then

$$\dot{\xi} = \begin{cases} \alpha V_\mathrm{F}, & \left|X - X_\mathrm{F}\right| < 1/2\alpha, \\ 0, & \left|X - X_\mathrm{F}\right| \ge 1/2\alpha. \end{cases} \tag{52}$$

The entropy production due to the reaction is given by Eq. (48), in which τ is the thickness of the reaction zone. The integral can be evaluated approximately using the rectangular midpoint rule:

$$\int_\tau A\dot{\xi}\,\mathrm{d}\tau = \int_{X_\mathrm{F}-1/2\alpha}^{X_\mathrm{F}+1/2\alpha} A\dot{\xi}\,\mathrm{d}X = \alpha^{-1}A\dot{\xi}\Big|_{X=X_\mathrm{F}} + O\left(\alpha^{-3}\right) = V_\mathrm{F}A + O\left(\alpha^{-3}\right). \tag{53}$$

Substituting ζ and μ_*, neglecting the dynamic terms (the terms with $\boldsymbol{v}$ and $\boldsymbol{j}$ can be considered to be small compared to the other terms in the case of quasistatics) and the last term of A (justification is given below), as well as the higher-order terms with respect to the width of the transition region, and denoting

$$\gamma = -\left.\frac{\partial f_\mathrm{C}}{\partial\phi}\right|_{X=X_\mathrm{F}} = -\left.\frac{\partial f_\mathrm{C}}{\partial\xi}\frac{\partial\xi}{\partial\phi}\right|_{X=X_\mathrm{F}}, \qquad \kappa = \left.\frac{\partial\phi}{\partial\xi}\right|_{X=X_\mathrm{F}} \tag{54}$$

leads to

$$\kappa V_\mathrm{F}\left(\gamma + \frac{\rho^0 n_*}{n_- M_-}\left(M_*\psi_* + p_*\frac{J}{c}\right) - [\![W]\!] + \boldsymbol{P} : [\![\boldsymbol{F}]\!]^\mathrm{T}\right) \ge 0, \tag{55}$$

where κ is the scalar multiplier.

It should be noted that neglecting the last term of A to obtain inequality (55) is justified due to the following reason. The last term of A is the Nabla operator acting on two separate terms: the derivative of f_C by $\nabla_0\xi$ and the term that is obtained directly from the last term of inequality (42). The latter is proportional to $\dot{\boldsymbol{N}}$, which is exactly zero for a non-rotating interface. The former transforms to $\Delta\xi$ in simple cases (as outlined in Section 3.1), which can be considered to be small at the centre of the transition zone, as the central point is close to the inflection point of the interface profile (it is exactly the inflection point in the case of a stationary interface, as seen from Eq. (61)).

2.7.2. The sharp-interface theory

The theory of the sharp-interface chemical reactions, which is based on the concept of the chemical affinity tensor, is summarised in Freidin and Vilchevskaya (2020). It has been shown that the entropy production due to the propagation of the chemical reaction front is

$$A_{NN}\omega[N] \ge 0, \tag{56}$$

where $\omega[N]$ is the reaction rate at the oriented surface element with normal $\boldsymbol{N}$. It is related to velocity V_F of the reaction front with respect to the reference configuration of the untransformed phase as

$$\omega[N] = \frac{\rho^0}{n_- M_-}V_\mathrm{F}. \tag{57}$$

Quantity A_{NN} is the normal component of a tensor referred to as the chemical affinity tensor, and, neglecting the dynamic terms, it is given by

$$A_{NN} = \frac{n_- M_-}{\rho^0}\left(\gamma - [\![W]\!] + \boldsymbol{P}_\pm : [\![\boldsymbol{F}]\!]^\mathrm{T} + p_+ J_+\right) + n_*\left(M_*\psi_* + M_*\frac{p_+}{\rho_*^0}J_+\right), \tag{58}$$

where the notation has been slightly changed to match the notation of the present paper. As in the sections above, ρ^0 is the mass density of the untransformed phase per unit volume of its reference configuration; n_- and n_* are the stoichiometric coefficients; M_- and M_* are the molar masses of the untransformed solid and the diffusing reactant, respectively; W_+ and W_- are the strain energy densities of the transformed and the untransformed phases, respectively, per unit volume of the reference configuration of the untransformed phase; $\boldsymbol{P}_\pm$ are the first Piola–Kirchhoff stress tensors defined in the reference configuration of the untransformed phase; $\boldsymbol{F}_\pm$ are the deformation gradients defined in the reference configuration of the untransformed phase; $J_+ = \det\boldsymbol{F}_+$ is the volume change of the transformed phase; ψ_* is the Helmholtz free energy per unit mass of the diffusing reactant; γ is the chemical energy. In addition to these quantities, p_+ denotes the pressure of the diffusing reactant.

Since $\boldsymbol{P}_{\pm} : [\![\boldsymbol{F}]\!]$ is equal to $\boldsymbol{P} : [\![\boldsymbol{F}]\!]$, which follows from Eqs. (29), (35) and (36), it can be seen that Eqs. (55) and (56) match almost exactly apart from two differences related to the pressure of the diffusing reactant. The first difference is the emergence of term $p_+\boldsymbol{J}_+$ in the first brackets in Eq. (58). The second difference is the presence of $p_+\boldsymbol{J}_+$ instead of $p_*\boldsymbol{J}$ in the second brackets in Eq. (58). There is also scalar multiplier κ in Eq. (55), which just acts as a time-scale multiplier.

The both pressure-related discrepancies are due to somewhat different problem formulations. In the model of the sharp-interface chemical reactions, it had been assumed that the diffusing reactant occupied only the volume of the transformed phase, i.e. it was only to one side of the interface, while the interface itself was not penetrable for the diffusing reactant. Therefore, the reactant applied pressure to the interface; hence, the balance of tractions at the interface contained the pressure term from the side of the transformed phase. In the present theory, the reaction taking place at a point is considered from the beginning, which is followed by construction of the RVE, in which the solid is divided into the transformed and the untransformed phases. Meanwhile, the pressure and the concentration of the diffusing reactant are still defined at the material point. Hence, the balance of tractions, Eq. (36), does not contain any terms related to the pressure of the diffusing reactant, which explains the first difference.

Furthermore, in the present theory, the diffusion through the material point is considered, and the chemical potential of the diffusing reactant contains material point quantities p_* and $\boldsymbol{J}$. In the sharp-interface theory, due to the diffusing reactant occupying only the transformed phase, the chemical potential of the diffusing reactant contains $p_+\boldsymbol{J}_+$ instead of $p_*\boldsymbol{J}$, explaining the second difference.

3. Numerical example

The aim of this section is to provide an illustrative example that gives rise to the localised reactions.

3.1. Motivation for chosen constitutive laws

The case of the reaction localisation is very similar to the classical stress-induced solid–solid phase transitions in the continuum. The only difference is the presence of the diffusion and the reaction in the former. Therefore, the latter is a good starting point for formulating the constitutive laws.

To describe smooth (finite-thickness) interfaces, traditionally, a field variable called "order parameter" is introduced, which indicates the phase at a material point (e.g. if it is close to 1 at point $\boldsymbol{x}$, then the point belongs to one phase, if it is close 0, then the point belongs to the other phase). The movement of the phase boundaries is then modelled as the evolution of the order parameter. Such approach is well-known and the theory underpinning it was first proposed by Ginzburg and Landau (1950). There are textbooks devoted to this topic (currently, it is commonly referred to as the "phase-field method"); therefore, only key points are highlighted below. A summary of the theory can be found in, e.g. Hohenberg and Krekhov (2015) and Qin and Bhadeshia (2010).

The simplest representation of the free energy density that gives rise to smooth phase boundaries has the following form:

$$f_{\mathrm{GL}} = f_0 + \frac{1}{2}B\,|\nabla\xi|^2 + f_1(\xi), \tag{59}$$

where ξ is the order parameter, f_0 and B are constants and $f_1(\xi)$ is some function of the order parameter that has two local minima. Different functions can be used, but it can be convenient to use the following expression:

$$f_1(\xi) = -K\cos^2(\pi\xi), \tag{60}$$

where K is a constant, as it allows constructing an analytical solution in the simplest case. It is easy to verify that in the case of 1D infinite domain, the following profile of the interface is formed:

$$\xi = \frac{1}{\pi}\arcsin\left(\tanh\left(\sqrt{\frac{2\pi^2 K}{B}}x\right)\right) + \frac{1}{2}, \tag{61}$$

where x is the spatial coordinate. In this case, $\sqrt{B/K}$ approximate the width of the interface.

In the 3D case, the evolution of the order parameter is governed by the following PDE:

$$\dot{\xi} = \nabla\cdot\frac{\partial f_{\mathrm{GL}}}{\partial\nabla\xi} - \frac{\partial f_{\mathrm{GL}}}{\partial\xi} = B\Delta\xi - \frac{\partial f_1}{\partial\xi}, \tag{62}$$

which is obtained via the functional derivative of the integral of the free energy density. Symbols ∇ and Δ denote the Nabla and the Laplace operators, while for the purpose of this section, the distinction between the configurations is not made.

Now, it is easy to see that for the existence of two phases, it is necessary for f_1 to have two local minima, where $\partial f_1/\partial\xi = 0$. Within each phase, ξ is almost homogeneous, $\Delta\xi$ becomes negligible and the right-hand side of Eq. (62) diminishes. Furthermore, for the phases to be stable, it is necessary that $\partial^2 f_1/\partial\xi^2 > 0$ in the neighbourhoods of the minima points of f_1. Otherwise, small perturbations of the right-hand side of Eq. (62) will lead to growth of $|\dot{\xi}|$, dislodging the order parameter from a local minimum.

It is also easy to see that for f_1 given by Eq. (60), the minima are achieved at $\xi = 0, 1$. Furthermore, Eq. (62) with such f_1 leads to stationary phase boundaries, i.e. when the correct profile of the interface is formed, $\dot{\xi}$ becomes zero. A driving force can be added to the system by amending f_1, for example,

$$f_1(\xi) = -K\cos^2(\pi\xi) + \frac{1}{2}\gamma\cos(\pi\xi), \tag{63}$$

where γ is a constant. In this case, the evolution of ξ is such that after the interface profile is formed, it moves with approximately constant velocity. For $\gamma > 0$, phase with $\xi = 1$ grows, while for $\gamma < 0$, the opposite takes place. It should be noted that K and γ cannot be arbitrary, as conditions on the second derivative of f_1 must be fulfilled for the phases to be stable.

3.2. Constitutive laws and simplified governing equations

For simplicity, a number of assumptions is made. First, the pressure of the diffusing reactant is neglected, $p_* = 0$, which corresponds to $W_* = 0$. Second, all mechanical terms that have dynamic nature are neglected in the linear momentum balance equation and in the chemical affinity. It should be noted that the wave propagation through phase-transformed layers described by phase-field-type models can also be studied as a separate problem, e.g. Rosi et al. (2013). Third, linear elasticity is considered, i.e. all non-linear terms related to the deformation are neglected. Although it is straightforward to rewrite the equations for the linear elastic case, it is useful to summarise the governing equations in this section.

Given the assumptions above, the linear momentum balance equation becomes

$$\nabla \cdot \boldsymbol{\sigma} = \mathbf{0}. \tag{64}$$

Following Eqs. (28), (29), (35) and (36), the Cauchy stress tensor is given by

$$\boldsymbol{\sigma} = \phi \boldsymbol{\sigma}_+ + (1-\phi)\,\boldsymbol{\sigma}_-, \tag{65}$$

where the following Cauchy stress tensors of the phases are introduced:

$$\boldsymbol{\sigma}_+ = {}^4\boldsymbol{C}_+ : \left(\boldsymbol{\varepsilon}_+ - \boldsymbol{\varepsilon}_{\mathrm{ch}}\right), \qquad \boldsymbol{\sigma}_- = {}^4\boldsymbol{C}_- : \boldsymbol{\varepsilon}_-, \tag{66}$$

where ${}^4\boldsymbol{C}_\pm$ are the stiffness tensors and $\boldsymbol{\varepsilon}_{\mathrm{ch}}$ is the chemical transformation strain tensor, which is considered to be constant (concentration-independent) for simplicity. The strain tensors of the phases are defined as

$$\boldsymbol{\varepsilon}_+ = \boldsymbol{\varepsilon} + \frac{1}{2}(1-\phi)\left(\boldsymbol{a}\boldsymbol{N} + \boldsymbol{N}\boldsymbol{a}\right), \qquad \boldsymbol{\varepsilon}_- = \boldsymbol{\varepsilon} - \frac{1}{2}\phi\left(\boldsymbol{a}\boldsymbol{N} + \boldsymbol{N}\boldsymbol{a}\right), \tag{67}$$

where $\boldsymbol{\varepsilon}$ is the infinitesimal linear strain tensor,

$$\boldsymbol{\varepsilon} = \frac{1}{2}\left(\nabla \boldsymbol{u} + (\nabla \boldsymbol{u})^{\mathrm{T}}\right), \tag{68}$$

where $\boldsymbol{u}$ is the displacement of a material point that is associated with the two-phase RVE, and $\boldsymbol{a}$ is found from

$$\boldsymbol{\sigma}_+ \cdot \boldsymbol{N} = \boldsymbol{\sigma}_- \cdot \boldsymbol{N}, \qquad \boldsymbol{N} = -\left|\nabla \phi\right|^{-1} \nabla \phi. \tag{69}$$

Thus, the total energy Helmholtz free energy density is

$$f = \phi w_+ + (1-\phi)\, w_- + f_{\mathrm{C}}, \tag{70}$$

where the linear-elastic strain energy densities for the phases are given by

$$w_+ = \frac{1}{2}\left(\boldsymbol{\varepsilon}_+ - \boldsymbol{\varepsilon}_{\mathrm{ch}}\right) : {}^4\boldsymbol{C}_+ : \left(\boldsymbol{\varepsilon}_+ - \boldsymbol{\varepsilon}_{\mathrm{ch}}\right), \qquad w_- = \frac{1}{2}\boldsymbol{\varepsilon}_- : {}^4\boldsymbol{C}_- : \boldsymbol{\varepsilon}_-, \tag{71}$$

and f_{C} will be given below.

Using the assumptions above, inequality (42) becomes

$$-\left(S + \frac{\partial f_{\mathrm{C}}}{\partial T}\right)\dot{T} - \boldsymbol{H}\cdot\frac{\nabla T}{T} - \frac{1}{M_*}\boldsymbol{j}\cdot\nabla\mu_* + \left(\mu_* - \frac{\partial f_{\mathrm{C}}}{\partial c}\right)\dot{c} + A\dot{\xi} - \phi\dot{w}_+ - (1-\phi)\,\dot{w}_- + \phi\boldsymbol{\sigma}_+ : \dot{\boldsymbol{\varepsilon}}_+ + (1-\phi)\,\boldsymbol{\sigma}_- : \dot{\boldsymbol{\varepsilon}}_- \geq 0, \tag{72}$$

where the simplified form of A will be given below. It is easy to see that the expressions for $w_\pm$ and $\boldsymbol{\sigma}_\pm$ satisfy inequality (72).

The following non-mechanical part of the free energy is assumed:

$$f_{\mathrm{C}} = f_0 + R_{\mathrm{g}}T\left(c\ln\frac{c}{c_0} - c\right) + \frac{1}{2}B\left|\nabla\xi\right|^2 - K\cos^2(\pi\xi) + \frac{1}{2}\gamma\cos(\pi\xi), \tag{73}$$

which consists of the Ginzburg–Landau part and the term depending on the concentration, where R_{g} is the universal gas constant and c_0 is some reference concentration. To satisfy inequality (72),

$$\mu_* = \frac{\partial f_{\mathrm{C}}}{\partial c} \tag{74}$$

is taken. It should be emphasised that for the purpose of this example, $\boldsymbol{\varepsilon}_{\mathrm{ch}}$ is taken to be constant; however, if it is concentration-dependent, Eq. (74) will contain deformation-dependent terms to satisfy inequality (72), as shown in, e.g. Poluektov and Figiel (2023). The second term of f_{C} results in the ideal gas chemical potential:

$$\mu_* = R_{\mathrm{g}}T\ln\frac{c}{c_0}. \tag{75}$$

Again, to satisfy inequality (72), $\boldsymbol{j}$ is chosen as

$$\boldsymbol{j} = -\frac{DM_*}{R_{\mathrm{g}}T}c\nabla\mu_*, \tag{76}$$

where D is the diffusivity parameter; however, it should be noted that more elaborate ways of choosing an expression for the diffusive flux exist (Bothe & Druet, 2023). Thus, the balance of mass becomes

$$\dot{c} = D\Delta c + \frac{\zeta}{M_*}\frac{\partial\phi}{\partial\xi}\dot{\xi}. \tag{77}$$

Following inequality (72), the (simplest) linear kinetics is chosen for the microstructural parameter:

$$\dot{\xi} = kA \qquad \text{for the case of phase transitions,} \tag{78}$$

$$\dot{\xi} = kcA \qquad \text{for the case of chemo-mechanics,} \tag{79}$$

where k is the kinetic constant and A is the chemical affinity. Two different equations are given to model two different cases: the first case is the classical stress-induced solid–solid phase transition problem, for which the diffusion problem is absent, the second case is the full chemo-mechanical problem. Given the assumptions above, the chemical affinity simplifies to

$$A = \frac{\partial \phi}{\partial \xi}\left(-\frac{\mu_* \zeta}{M_*} - [\![w]\!] + \boldsymbol{\sigma} : [\![\boldsymbol{\varepsilon}]\!]\right) - \frac{\partial f_{\mathrm{C}}}{\partial \xi} + \nabla \cdot \frac{\partial f_{\mathrm{C}}}{\partial \nabla \xi} - A_{\mathrm{I}}, \tag{80}$$

$$A_{\mathrm{I}} = \nabla \cdot \left(\phi(1-\phi)\,\boldsymbol{a} \cdot [\![\boldsymbol{\sigma}]\!]\left|\nabla_0 \xi\right|^{-1}\right). \tag{81}$$

It should be noted that A_{I} will contain higher-order gradients of $\boldsymbol{u}$, i.e. $\nabla\nabla\boldsymbol{u}$, which can be neglected for consistency with the other equations written for the case of linear elasticity.

Finally, it is necessary to specify an expression for $\phi(\xi)$. It can be seen that Eqs. (78)–(79) have similar structure to Eq. (62). However, certain care must be taken for these equations to describe two distinct phases — the right-hand side of Eqs. (78)–(79) should be zero when $\xi = 0, 1$, otherwise, the bulk phases will start evolving. On top of that, $\phi(\xi)$ should be monotonically increasing and $\phi = 0, 1$ at $\xi = 0, 1$, respectively, to preserve the physical meaning of the microstructural parameter, which is the indication of the degree of the transformation of the material microstructure. Choosing relation

$$\phi = \frac{1}{2}\left(1 - \cos(\pi\xi)\right) \tag{82}$$

satisfies these requirements. In particular, $\partial\phi/\partial\xi = 0$ at $\xi = 0, 1$, leading to $A = 0$ within the bulk phases.

To summarise, the considered full chemo-mechanical problem consists in solving the system of coupled PDEs (64), (77) and (79) with respect to unknown fields $\boldsymbol{u}(\boldsymbol{x}, t)$, $c(\boldsymbol{x}, t)$ and $\xi(\boldsymbol{x}, t)$, given some boundary and some initial conditions. A particular case of this problem is the stress-induced solid–solid phase transition problem that consists in solving the system of coupled PDEs (64) and (78) with respect to unknown fields $\boldsymbol{u}(\boldsymbol{x}, t)$ and $\xi(\boldsymbol{x}, t)$, while $\mu_* = 0$ in Eq. (80) indicating that there is no diffusive species.

3.3. Numerical results

To illustrate the theory, a 1D example is considered. Thus, $\boldsymbol{u} = u_x \boldsymbol{e}_x$. The domain of length L is considered. Planar chemical strain is assumed:

$$\boldsymbol{\varepsilon}_{\mathrm{ch}} = \theta\left(\boldsymbol{I} - \boldsymbol{e}_z \boldsymbol{e}_z\right), \tag{83}$$

where θ is a constant. Isotropic elasticity is taken:

$${}^4\boldsymbol{C}_{\pm} = \lambda_{\pm} \boldsymbol{I}\boldsymbol{I} + 2\mu_{\pm}\,{}^4\boldsymbol{\mathcal{I}}, \tag{84}$$

where $\lambda_{\pm}$ and $\mu_{\pm}$ are the Lamé parameters, ${}^4\boldsymbol{\mathcal{I}}$ is the fourth-order unit tensor for second-order symmetric tensors, which in Cartesian coordinates is $\mathcal{I}_{ijkl} = \left(\delta_{ik}\delta_{jl} + \delta_{il}\delta_{jk}\right)/2$.

Due to the 1D nature of the problem, $[\![\boldsymbol{\varepsilon}]\!] = a\boldsymbol{e}_x\boldsymbol{e}_x$ and $\boldsymbol{N} = \boldsymbol{e}_x$; therefore, $\boldsymbol{a} = a\boldsymbol{e}_x$, and, consequently, $A_{\mathrm{I}} = 0$. For the mechanical problem, $u_x = 0$ at $x = 0$ and $u_x = u_0$ at $x = L$ are enforced. For the diffusion problem,

$$-D\frac{\partial c}{\partial x} + \alpha\left(c - c_0\right) = 0 \qquad \text{at } x = 0, \qquad \frac{\partial c}{\partial x} = 0 \qquad \text{at } x = L, \tag{85}$$

are enforced, where α is the surface mass transfer coefficient. For the evolution of the order parameter, $\partial\xi/\partial x = 0$ at $x = 0, L$ is enforced. Initial concentration $c = c_{\mathrm{i}}$ at $t = 0$ is assumed for the entire domain. The following initial profile is assumed for ξ:

$$\xi = -\frac{1}{\pi}\arcsin\left(\tanh\left(\sqrt{\frac{2\pi^2 K}{B}}\left(x - x_{0\mathrm{i}}\right)\right)\right) + \frac{1}{2}, \tag{86}$$

where $x_{0\mathrm{i}}$ is the initial position of the centre of the interface. The equations are solved using the explicit finite-difference method (second-order in space, first-order in time) on a regular grid with spatial size Δx and time step Δt.

3.3.1. Phase transition

As pointed out earlier, the case of the localised reactions is very similar to the stress-induced solid–solid phase transitions — the difference is the presence of the diffusion. The numerical examples of the present paper serve the purpose of providing illustrations/clarifications to the theory; thus, the most simple scenario is demonstrated first — the phase transition problem. It is used to show the effect of the stresses on the kinetics of the interface. Moreover, first, the case of zero transformation strain is considered (hence, zero stresses), which gives obvious interface kinetics — constant velocity of the front. Then, some transformation strain is assumed, giving rise to the stresses, which affect the front kinetics. This scenario is intended to help the reader to understand better the chemo-mechanical problem presented in the subsequent subsection.

For the purpose of the paper, the units of the quantities are omitted. The following problem parameters are taken: $L = 20$, $B = K = 0.02$, $k = 1$, $\gamma = 0.05$, $\lambda_+ = 50$, $\lambda_- = 10$, $\mu_+ = 58$, $\mu_- = 26$ and $x_{0\mathrm{i}} = 4$. Numerical parameters $\Delta x = L/400$ and

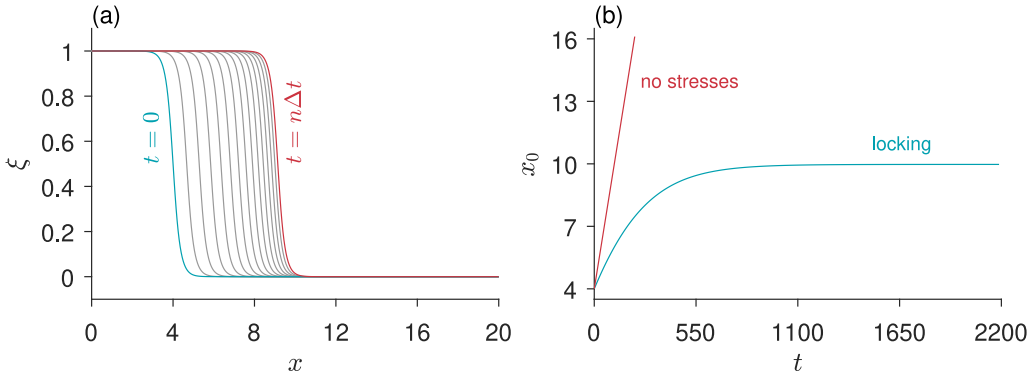

Fig. 2. The interface profile as a function of the spatial coordinate at different moments of time for the "locking" scenario (a). Grey lines correspond to each 750th time step, $n = 10500$. The dependence of the interface position on time (b).

$\Delta t = 0.7\Delta x^2/2B$ are taken, ensuring that the CFL condition is not violated. For the mechanical part of the problem, two different scenarios are considered: "locking" with $\theta = 0.005$ and $u_0 = 0.0453L$, "no stresses" with $\theta = 0$ and $u_0 = 0$. The first scenario corresponds to the case when the interface should be blocked by the stresses exactly at the centre of the computational domain; therefore, the quoted value of parameter u_0 was obtained by solving $A = 0$ with respect to u_0 at $x_0 = L/2$, where x_0 denotes the coordinate of the centre of the interface (i.e. when $\xi = 0.5$), taking the sharp-interface limit. The second scenario corresponds to the case when there is no transformation strain and no displacements are applied to the material boundary; hence, the stresses and the strains are exactly zero.

In Fig. 2a, the dynamics of the interface profile for the "locking" scenario is demonstrated. Fig. 2b shows the evolution of the centre of the interface and it can be seen that, in the case when the stresses are present, the propagation of the interface is slowed down as it approaches the equilibrium position at $x = 10$. In the case when the stresses are absent, the centre of the interface moves with the constant velocity, as is expected from this model.

3.3.2. Chemo-mechanics

In the chemo-mechanical problem, there is the combined effect of the concentration and the stresses on the kinetics of the interface. In addition to the parameters quoted in the previous subsection, the following problem parameters related to the diffusion are taken: $D = \alpha = 0.02$, $c_0 = 1$, $\zeta/M_* = -1$, $R_gT = 10^{-3}$, $c_i = 10^{-10}$. Again, for the mechanical part of the problem "locking" and "no stresses" scenarios are considered.

In contrast to the phase transition example, now, the interface can only move by the consumption of the diffusive species. In Figs. 3a and 3b, it can be seen that in the "locking" scenario, the interface behaves similarly to the previous example. However, in the case when the stresses are absent, the centre of the interface moves parabolically as a function of time, indicating that the process is diffusion-controlled. The dynamics of the concentration profile for both scenarios is shown in Figs. 3c and 3d, where it can be seen that when the stresses are absent, the diffusion profile decays in space down to a small value at the interface and most of the diffusive species is consumed for the interface propagation — almost no amount of the diffusive species propagates past the interface. In this case, the diffusion governs the interface propagation. When the stresses are present, they slow down and block the interface propagation, while the diffusion process still takes palace. Therefore, at the initial stages, a kink in the concentration profile can be seen at the interface position, with only a small amount of the diffusive species going past the interface. As the interface slows down, a larger amount of the diffusive species goes into the chemically untransformed phase, gradually increasing the concentration there. It should be noted that there is a visual jump between the blue line and the first grey line in Figs. 3c and 3d because at the initial time steps, the diffusion takes place significantly more rapidly than subsequently. Furthermore, one can notice small 'acceleration' regime around $t = 0$ in Fig. 3b that is related to the absence of the concentration of the diffusive species initially, which is necessary for the interface propagation.

4. Conclusions

The present paper proposes a thermo-chemo-mechanical theory, which describes the diffusion of mobile species through the solid and the mass exchange between them via the chemical reaction. The diffusion and the reaction can lead to the emergence of the transformation strains, which, in turn, affect the kinetics of the described processes. The thermodynamically-consistent theory has been derived from the mass, momentum, energy and entropy balances. It has been shown that by constructing a two-phase material point description, it is possible to obtain (in the limit) the same driving force for the chemical reaction (hence, the same reaction kinetics) as derived within the theory of the sharp-interface chemical reactions. The derived theory has been used within two computational examples comparing chemo-mechanics and solid–solid phase transitions. The resulting theory can provide an alternative approach to modelling of the localised stress-affected chemical reactions in solids when researchers would like to avoid using computational techniques resolving the sharp-interface kinetics and prefer resolving the PDE governing the evolution of the reaction extent.

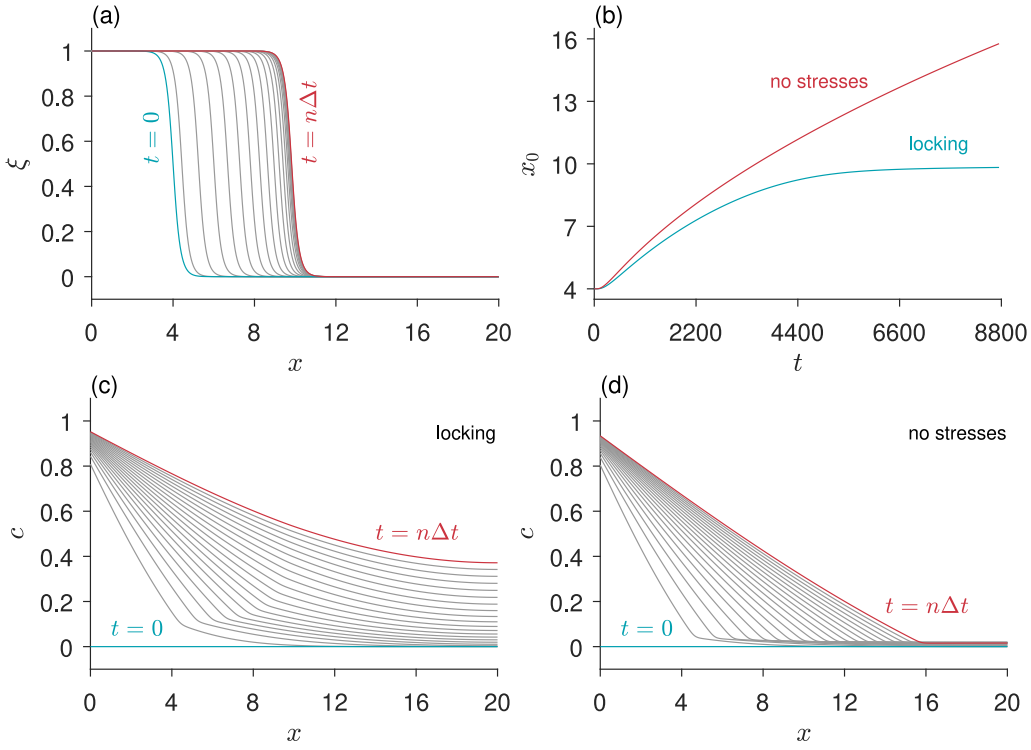

Fig. 3. The interface profile as a function of the spatial coordinate at different moments of time for the "locking" scenario (a). Grey lines correspond to each 10^4th time step, $n = 2 \cdot 10^5$. The dependence of the interface position on time (b). The concentration profile as a function of the spatial coordinate at different moments of time for the "locking" scenario (c) and the "no stresses" scenario (d).

CRediT authorship contribution statement

Michael Poluektov: Conceptualization, Formal analysis, Software, Visualization, Writing – original draft, Writing – review & editing. **Alexander B. Freidin:** Conceptualization, Formal analysis, Writing – review & editing.

Declaration of competing interest

The authors declare the following financial interests/personal relationships which may be considered as potential competing interests: ABF reports that the financial support was provided by the Russian Science Foundation.

Acknowledgements

ABF acknowledges the support of the Russian Science Foundation (Grant No. 19-19-00552-Π)

References

Anguiano, M., Masud, A., & Rajagopal, K. R. (2022). Mixture model for thermo-chemo-mechanical processes in fluid-infused solids. *International Journal of Engineering Science*, *174*, Article 103576. http://dx.doi.org/10.1016/j.ijengsci.2021.103576.

Bothe, D., & Druet, P.-É. (2023). On the structure of continuum thermodynamical diffusion fluxes — A novel closure scheme and its relation to the Maxwell–Stefan and the Fick–Onsager approach. *International Journal of Engineering Science*, *184*, Article 103818. http://dx.doi.org/10.1016/j.ijengsci.2023.103818.

Bower, A. F., Guduru, P. R., & Sethuraman, V. A. (2011). A finite strain model of stress, diffusion, plastic flow, and electrochemical reactions in a lithium-ion half-cell. *Journal of the Mechanics and Physics of Solids*, *59*, 804–828. http://dx.doi.org/10.1016/j.jmps.2011.01.003.

Büttner, C. C., & Zacharias, M. (2006). Retarded oxidation of Si nanowires. *Applied Physics Letters*, *89*, Article 263106. http://dx.doi.org/10.1063/1.2424297.

Coleman, B. D., & Noll, W. (1963). The thermodynamics of elastic materials with heat conduction and viscosity. *Archive for Rational Mechanics and Analysis*, *13*, 167–178. http://dx.doi.org/10.1007/BF01262690.

Cui, Z. W., Gao, F., & Qu, J. M. (2012). A finite deformation stress-dependent chemical potential and its applications to lithium ion batteries. *Journal of the Mechanics and Physics of Solids*, *60*, 1280–1295. http://dx.doi.org/10.1016/j.jmps.2012.03.008.

Cui, Z. W., Gao, F., & Qu, J. M. (2013). Interface–reaction controlled diffusion in binary solids with applications to lithiation of silicon in lithium-ion batteries. *Journal of the Mechanics and Physics of Solids*, *61*, 293–310. http://dx.doi.org/10.1016/j.jmps.2012.11.001.

Drozdov, A. D. (2014). Viscoplastic response of electrode particles in Li-ion batteries driven by insertion of lithium. *International Journal of Solids and Structures*, *51*, 690–705.

Drozdov, A. D. (2018). Mechanical behavior of temperature-sensitive gels under equilibrium and transient swelling. *International Journal of Engineering Science*, *128*, 79–100. http://dx.doi.org/10.1016/j.ijengsci.2018.03.009.

Eremeyev, V. A., Rosi, G., & Naili, S. (2019). Comparison of anti-plane surface waves in strain-gradient materials and materials with surface stresses. *Mathematics and Mechanics of Solids*, *24*, 2526–2535. http://dx.doi.org/10.1177/1081286518769960.

Evstafeva, I., & Pronina, Y. (2023). On the mechanochemical dissolution of shells and its temperature dependence: Discussion of different models. *International Journal of Engineering Science*, *190*, Article 103889. http://dx.doi.org/10.1016/j.ijengsci.2023.103889.

Freidin, A. B. (2013). Chemical affinity tensor and stress-assist chemical reactions front propagation in solids. In *Mechanics of Solids, Structures and Fluids*: *Vol. 9*, *ASME International Mechanical Engineering Congress and Exposition*. http://dx.doi.org/10.1115/IMECE2013-64957, V009T10A102.

Freidin, A. B., & Vilchevskaya, E. N. (2020). Chemical affinity tensor in coupled problems of mechanochemistry. In H. Altenbach, & A. Öchsner (Eds.), *Encyclopedia of continuum mechanics*. Springer Berlin Heidelberg, http://dx.doi.org/10.1007/978-3-662-53605-6_143-1.

Freidin, A. B., Vilchevskaya, E. N., & Korolev, I. K. (2014). Stress-assist chemical reactions front propagation in deformable solids. *International Journal of Engineering Science*, *83*, 57–75. http://dx.doi.org/10.1016/j.ijengsci.2014.03.008.

Ge, S., Ma, Y., Wang, K., Zheng, L., Xie, X., Chen, X., & Yu, H.-S. (2023). Unsaturated hydro-mechanical-electro-chemical coupling based on mixture-coupling theory: A unified model. *International Journal of Engineering Science*, *191*, Article 103914. http://dx.doi.org/10.1016/j.ijengsci.2023.103914.

Ginzburg, V. L., & Landau, L. D. (1950). K teorii sverhprovodimosti. *Zhurnal Eksperimentalnoi i Teoreticheskoi Fiziki*, *20*, 1064.

Glansdorff, P., & Prigogine, I. (1971). *Thermodynamic theory of structure, stability and fluctuations*. John Wiley & Sons Ltd.

Gomez-Constante, J. P., Pagilla, P. R., & Rajagopal, K. R. (2021). A thermomechanical and photochemical description of the phase change process in roll-to-roll nanoimprinting lithography. *International Journal of Engineering Science*, *169*, Article 103564. http://dx.doi.org/10.1016/j.ijengsci.2021.103564.

Gutman, E. M. (1994). *Mechanochemistry of solid surfaces*. World Scientific, http://dx.doi.org/10.1142/2373.

Hohenberg, P. C., & Krekhov, A. P. (2015). An introduction to the Ginzburg–Landau theory of phase transitions and nonequilibrium patterns. *Physics Reports*, *572*, 1–42. http://dx.doi.org/10.1016/j.physrep.2015.01.001.

Knyazeva, A. G. (2003). Cross effects in solid media with diffusion. *Journal of Applied Mechanics and Technical Physics*, *44*, 373–384.

Levitas, V. I., & Attariani, H. (2014). Anisotropic compositional expansion in elastoplastic materials and corresponding chemical potential: Large-strain formulation and application to amorphous lithiated silicon. *Journal of the Mechanics and Physics of Solids*, *69*, 84–111. http://dx.doi.org/10.1016/j.jmps.2014.04.012.

Liu, X. H., Zheng, H., Zhong, L., Huan, S., Karki, K., Zhang, L. Q., Liu, Y., Kushima, A., Liang, W. T., Wang, J. W., Cho, J. H., Epstein, E., Dayeh, S. A., Picraux, S. T., Zhu, T., Li, J., Sullivan, J. P., Cumings, J., Wang, C. S., ... Huang, J. Y. (2011). Anisotropic swelling and fracture of silicon nanowires during lithiation. *Nano Letters*, *11*, 3312–3318. http://dx.doi.org/10.1021/nl201684d.

Loeffel, K., & Anand, L. (2011). A chemo-thermo-mechanically coupled theory for elastic-viscoplastic deformation, diffusion, and volumetric swelling due to a chemical reaction. *International Journal of Plasticity*, *27*, 1409–1431. http://dx.doi.org/10.1016/j.ijplas.2011.04.001.

Loeffel, K., Anand, L., & Gasem, Z. M. (2013). On modeling the oxidation of high-temperature alloys. *Acta Materialia*, *61*, 399–424. http://dx.doi.org/10.1016/j.actamat.2012.07.067.

McDowell, M. T., Lee, S. W., Harris, J. T., Korgel, B. A., Wang, C. M., Nix, W. D., & Cui, Y. (2013). In situ TEM of two-phase lithiation of amorphous silicon nanospheres. *Nano Letters*, *13*, 758–764. http://dx.doi.org/10.1021/nl3044508.

McDowell, M. T., Lee, S. W., Nix, W. D., & Cui, Y. (2013). 25th anniversary article: Understanding the lithiation of silicon and other alloying anodes for lithium-ion batteries. *Advanced Materials*, *25*, 4966–4984. http://dx.doi.org/10.1002/adma.201301795.

Morozov, A., Freidin, A. B., & Müller, W. H. (2023). On stress-affected propagation and stability of chemical reaction fronts in solids. *International Journal of Engineering Science*, *189*, Article 103876. http://dx.doi.org/10.1016/j.ijengsci.2023.103876.

Poluektov, M., & Figiel, Ł. (2023). A two-scale framework for coupled mechanics-diffusion-reaction processes. *International Journal of Solids and Structures*, *279*, Article 112386. http://dx.doi.org/10.1016/j.ijsolstr.2023.112386.

Poluektov, M., Freidin, A. B., & Figiel, Ł. (2018). Modelling stress-affected chemical reactions in non-linear viscoelastic solids with application to lithiation reaction in spherical Si particles. *International Journal of Engineering Science*, *128*, 44–62. http://dx.doi.org/10.1016/j.ijengsci.2018.03.007.

Pronina, Y. (2017). An analytical solution for the mechanochemical growth of an elliptical hole in an elastic plane under a uniform remote load. *European Journal of Mechanics-A/Solids*, *61*, 357–363. http://dx.doi.org/10.1016/j.euromechsol.2016.10.009.

Pronina, Y. G., & Khryashchev, S. M. (2017). Mechanochemical growth of an elliptical hole under normal pressure. *Materials Physics and Mechanics*, *31*, 52–55.

Pronina, Y., Sedova, O., Grekov, M., & Sergeeva, T. (2018). On corrosion of a thin-walled spherical vessel under pressure. *International Journal of Engineering Science*, *130*, 115–128. http://dx.doi.org/10.1016/j.ijengsci.2018.05.004.

Qin, R. S., & Bhadeshia, H. K. (2010). Phase field method. *Materials Science and Technology*, *26*, 803–811. http://dx.doi.org/10.1179/174328409X453190.

Qin, B., & Zhong, Z. (2021). A theoretical model for thermo-chemo-mechanically coupled problems considering plastic flow at large deformation and its application to metal oxidation. *International Journal of Solids and Structures*, *212*, 107–123. http://dx.doi.org/10.1016/j.ijsolstr.2020.12.006.

Rao, V. S., & Hughes, T. J. R. (2000). On modelling thermal oxidation of silicon I: Theory. *International Journal for Numerical Methods in Engineering*, *47*, 341–358. http://dx.doi.org/10.1002/(SICI)1097-0207(20000110/30)47:1/3<341.

Rosi, G., Giorgio, I., & Eremeyev, V. A. (2013). Propagation of linear compression waves through plane interfacial layers and mass adsorption in second gradient fluids. *Zeitschrift für Angewandte Mathematik und Mechanik*, *93*, 914–927. http://dx.doi.org/10.1002/zamm.201200285.

Schneider, D., Schwab, F., Schoof, E., Reiter, A., Herrmann, C., Selzer, M., Böhlke, T., & Nestler, B. (2017). On the stress calculation within phase-field approaches: A model for finite deformations. *Computational Mechanics*, *60*, 203–217. http://dx.doi.org/10.1007/s00466-017-1401-8.

Schneider, D., Tschukin, O., Choudhury, A., Selzer, M., Böhlke, T., & Nestler, B. (2015). Phase-field elasticity model based on mechanical jump conditions. *Computational Mechanics*, *55*, 887–901. http://dx.doi.org/10.1007/s00466-015-1141-6.

Sedova, O., & Pronina, Y. (2022). The thermoelasticity problem for pressure vessels with protective coatings, operating under conditions of mechanochemical corrosion. *International Journal of Engineering Science*, *170*, Article 103589. http://dx.doi.org/10.1016/j.ijengsci.2021.103589.

Serpelloni, M., Arricca, M., Bonanno, C., & Salvadori, A. (2022). Chemo-transport-mechanics in advecting membranes. *International Journal of Engineering Science*, *181*, Article 103746. http://dx.doi.org/10.1016/j.ijengsci.2022.103746.

Soleimani, K., Ghasemloonia, A., & Sudak, L. (2023). Theory of porous media with the advection term and mass exchange between phases. *International Journal of Engineering Science*, *191*, Article 103915. http://dx.doi.org/10.1016/j.ijengsci.2023.103915.

Sreejith, P., Kannan, K., & Rajagopal, K. R. (2023). A thermodynamic framework for the additive manufacturing of crystallizing polymers. Part I: A theory that accounts for phase change, shrinkage, warpage and residual stress. *International Journal of Engineering Science*, *183*, Article 103789. http://dx.doi.org/10.1016/j.ijengsci.2022.103789.

Tschukin, O., Schneider, D., & Nestler, B. (2019). An elasto-chemical phase-field model for isotropic solids. *European Journal of Mechanics-A/Solids*, *73*, 181–191. http://dx.doi.org/10.1016/j.euromechsol.2018.06.014.

de Vasconcelos, L. S., Xu, R., Xu, Z., Zhang, J., Sharma, N., Shah, S. R., Han, J., He, X., Wu, X., Sun, H., Hu, S., Perrin, M., Wang, X., Liu, Y., Lin, F., Cui, Y., & Zhao, K. (2022). Chemomechanics of rechargeable batteries: Status, theories, and perspectives. *Chemical Reviews*, *122*, 13043–13107. http://dx.doi.org/10.1021/acs.chemrev.2c00002.

Yang, F., Li, Y., & Zhang, K. (2023). A multiplicative finite strain deformation for diffusion-induced stress: An incremental approach. *International Journal of Engineering Science*, *187*, Article 103841. http://dx.doi.org/10.1016/j.ijengsci.2023.103841.